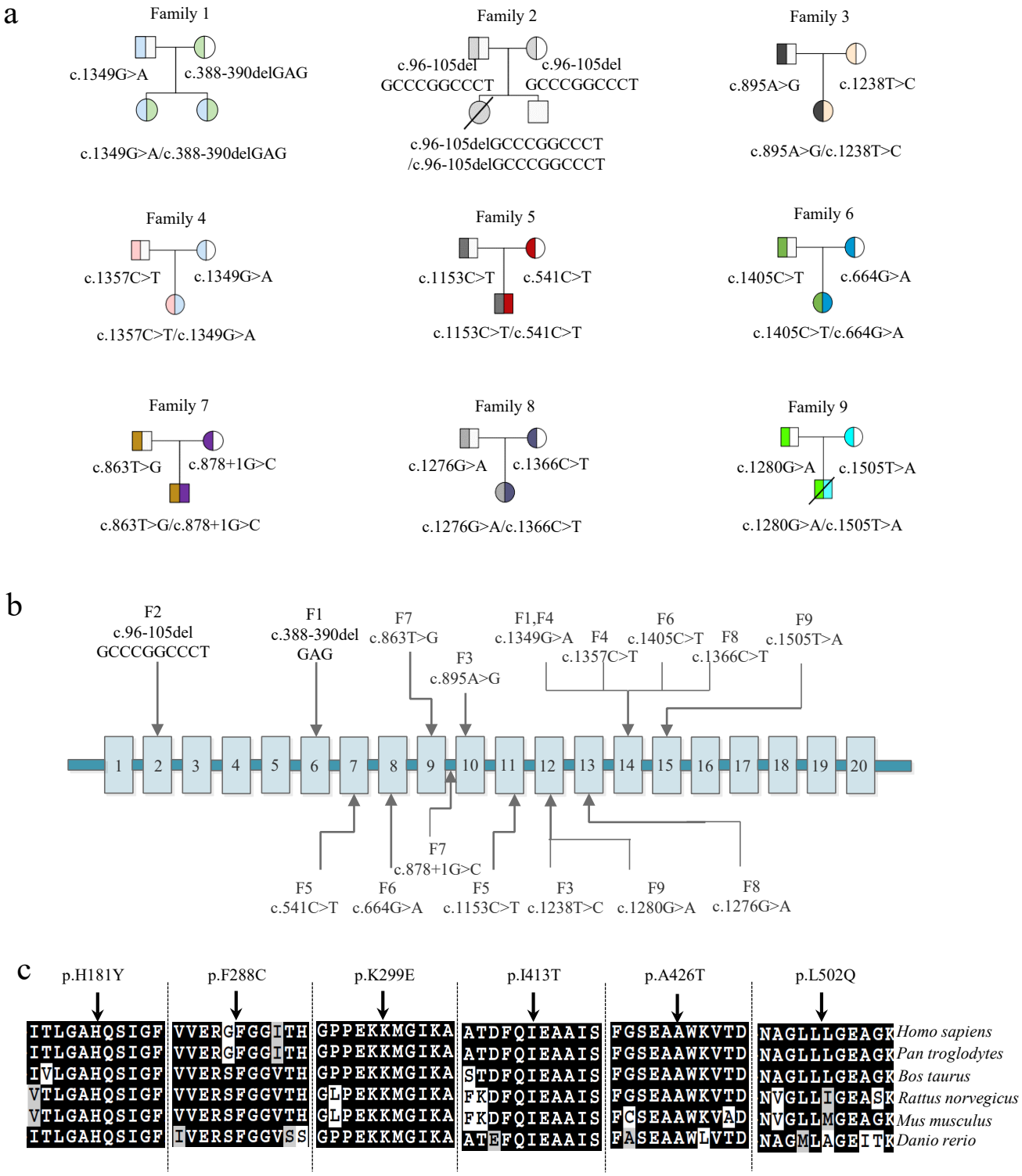


Fig S1. Variants in VLCAD-deficient patients and their conservative analysis.
(a) Genotypes of VLCAD deficiency pedigrees; (b) Variants distribution in *ACADVL*; (c) Conservative analysis of six novel missense variants in species (*Homo sapiens*, *NP_000009.1*; *Pan troglodytes, XP_016786900.1*; *Bos Taurus, NP_776919.1*; *Ratus norvegicus, NP_037023.1*; *Mus musculus, NP_059062.1*; *Danio rerio, NP_997776.1*)

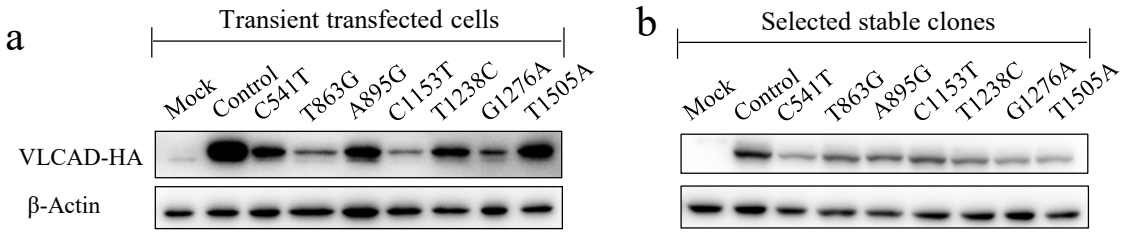


Fig S2. Expression levels of HA-tagged VLCAD in cells. (a) transient transfected cells and (b) the stable cells. β-Actin is used as a loading control on the same blot.

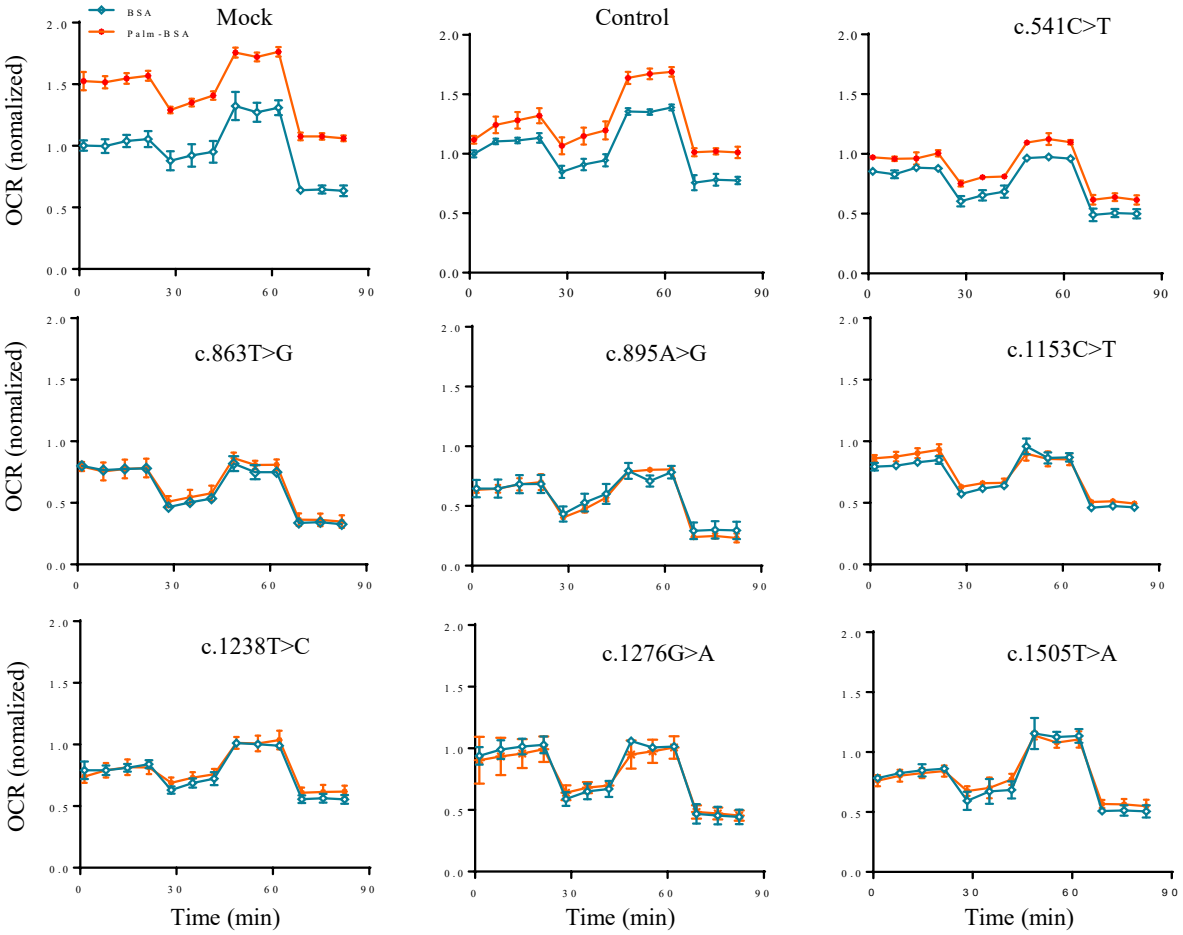


Fig S3. FAO capacity for utilization of exogenous palmitate. Oxygen-consumption rate (OCR) was monitored by sequential injections of oligomycin, FCCP, antimycin A and rotenone (downward arrows) in the presence of bovine serum albumin alone (BSA) or conjugated to palmitate (Palm-BSA).

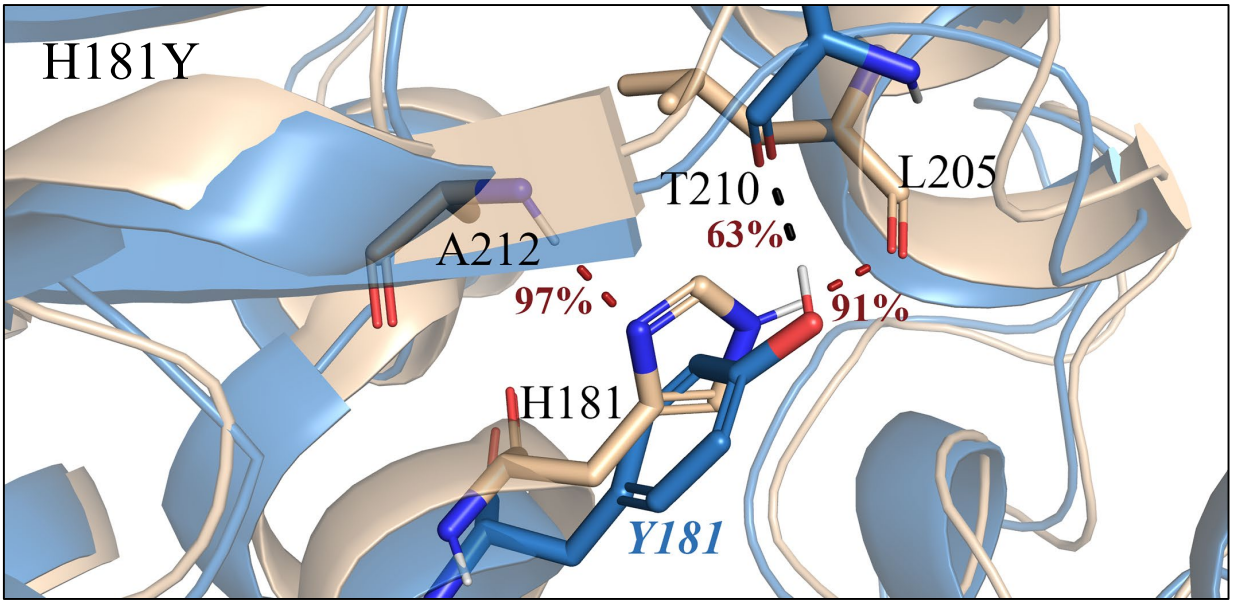
H181Y
T210
L205
63%
A212
97%
91%
H181
Y181

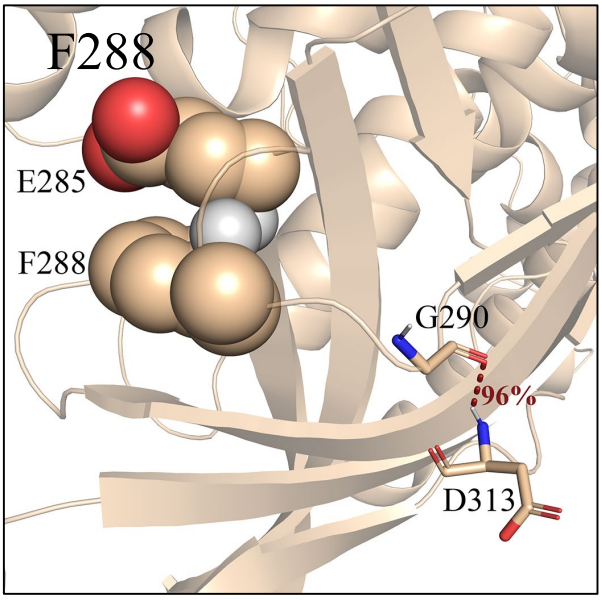
F288
E285
F288
G290
96%
D313

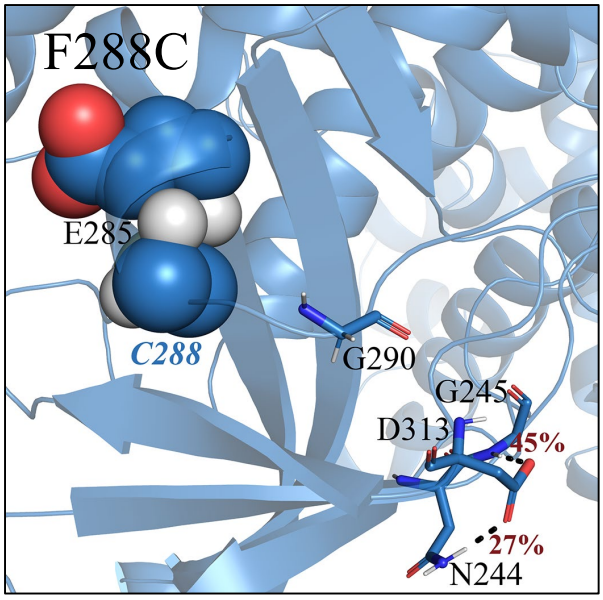
F288C
E285
C288
G290
G245
D313
45%
27%
N244

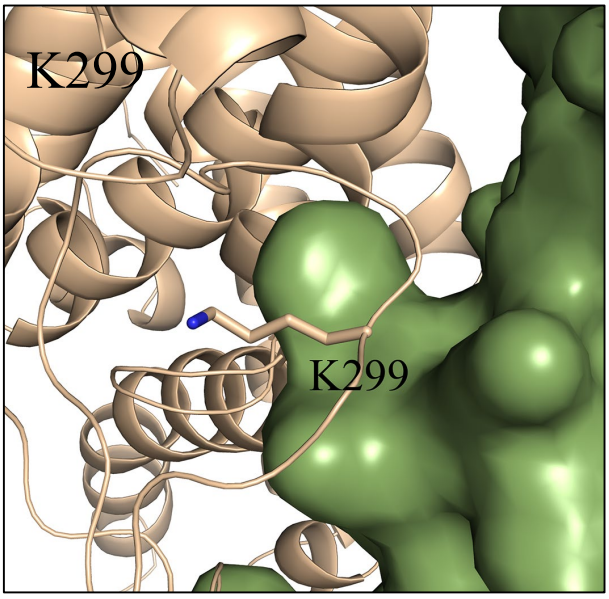
K299
K299

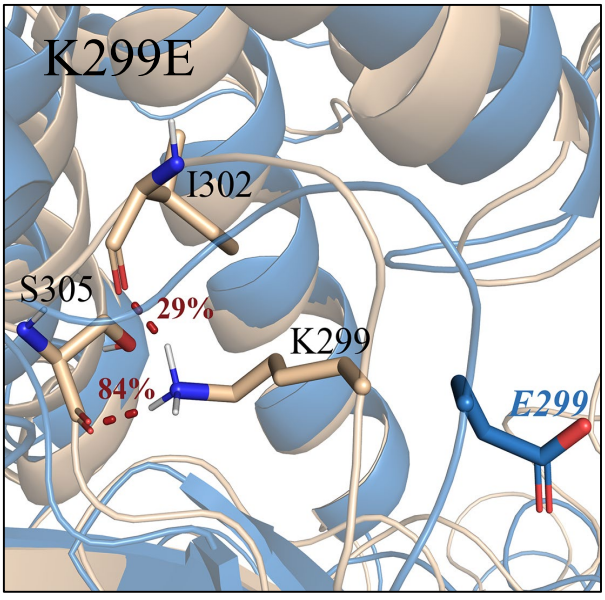
K299E
I302
S305
29%
K299
84%
E299

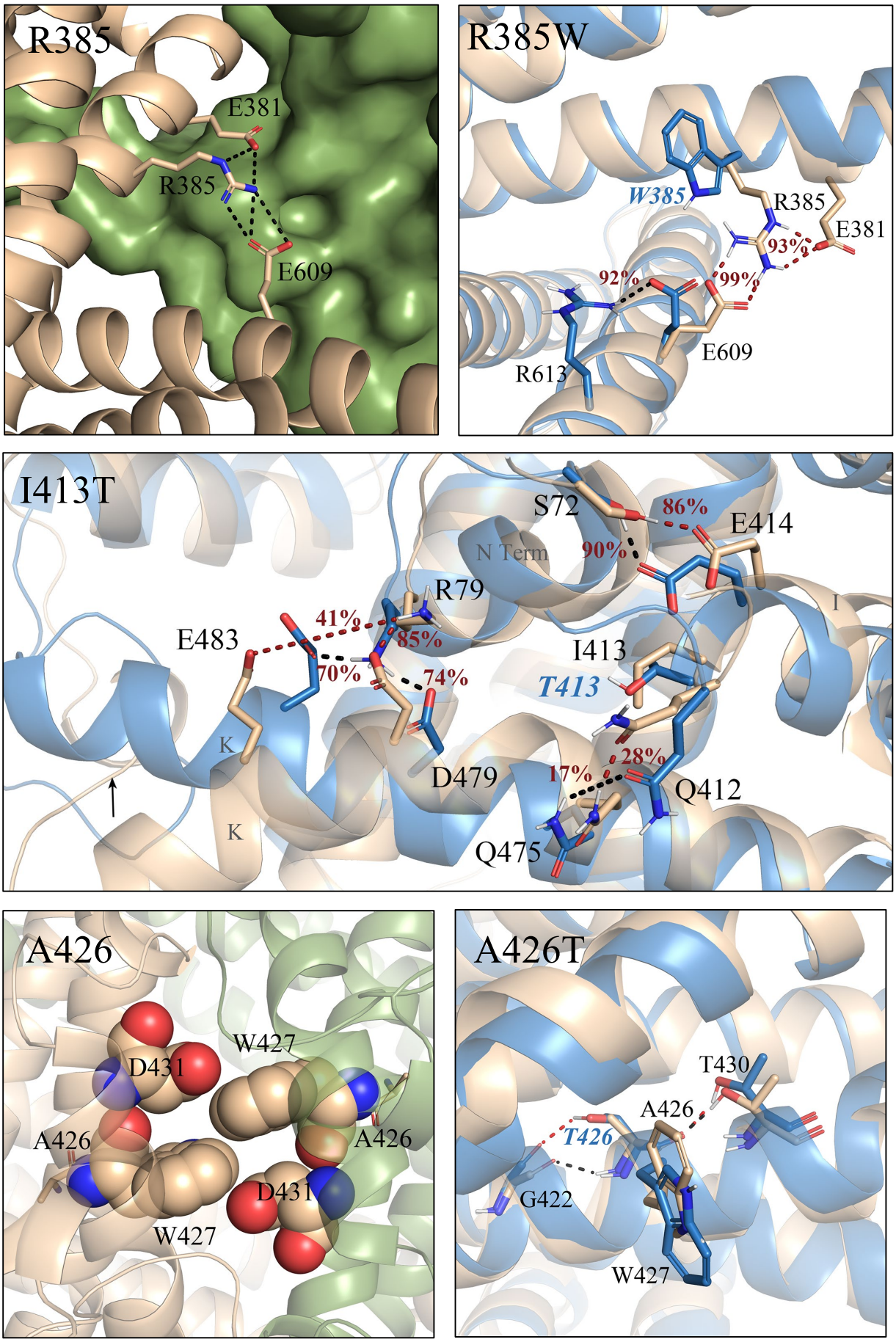


Fig. S4 Structural predictions in wild-type and mutant residues. The structure of the mutant was shown in sky blue with the WT in tan or green. The black and red dashed represent the electrostatic interactions of mutant and WT, respectively. The occupancy of the hydrogen bonds was shown in red.